Novel 3D printed device with integrated macroscale magnetic field triggerable anti-cancer drug delivery system

Article (Accepted Version)

Novel 3D printed device with integrated macroscale magnetic field triggerable anti-cancer drug delivery system

Kejing Shi[1], Rodrigo Aviles-Espinosa[2], Elizabeth Rendon-Morales[2], Lisa Woodbine[3], Mohammed Maniruzzaman[4,*], Ali Nokhodchi[1,*]

[1]Pharmaceutics Research Laboratory, School of Life Sciences, University of Sussex, Falmer, Brighton, BN1 9QJ, UK;[2]Robotics and Mechatronics Systems Research Centre, School of Engineering and Informatics, University of Sussex, Falmer, Brighton, BN1 9RH, UK;[3]Sussex Centre for Genome Damage and Stability, School of Life Sciences, University of Sussex, Falmer, Brighton, BN1 9RQ, UK;[4]Pharmaceutical Engineering and 3D Printing Lab, Division of Molecular Pharmaceutics and Drug Delivery, College of Pharmacy, The University of Texas at Austin, 2409 University Avenue, Austin, TX 78712, USA

***corresponding authors:**

Ali Nokhodchi; e-mail:a.nokhodchi@sussex.ac.uk; Tel: +44 1273872811

Mohammad Maniruzzaman; e-mail: M.Maniruzzaman@austin.utexas.edu; Tel: +1-512-232-4743

Total number of words including references: 6419

Total number of Figures 7

Total number of Tables 1

Abstract:

With the growing demand for personalized medicine and medical devices, the impact of on-demand triggerable (e.g., via magnetic fields) drug delivery systems increased significantly in recent years. The three-dimensional (3D) printing technology has already been applied in the development of personalized dosage forms because of its high-precision and accurate manufacturing ability. In this study, a novel magnetically triggerable drug delivery device composed of a magnetic polydimethylsiloxane (PDMS) sponge cylinder and a 3D printed reservoir was designed, fabricated and characterized. This system can realize a switch between "on" and "off" state easily through the application of different magnetic fields and from different directions. Active and repeatable control of the localized drug release could be achieved by the utilization of magnetic fields to this device due to the shrinking extent of the macro-porous magnetic sponge inside. The switching "on" state of drug-releasing could be realized by the magnetic bar contacted with the side part of the device because the times at which 50%, 80% and 90% (w/w) of the drug were dissolved are observed to be 20, 55 and 140 min, respectively. In contrast, the switching "off" state of drug-releasing could be realized by the magnetic bar placed at the bottom of the device as only 10% (w/w) of the drug could be released within 12 h. An anti-cancer substance, 5-fluorouracil (FLU), was used as the model drug to illustrate the drug release behaviour of the device under different strengths of magnetic fields applied. *In vitro* cell culture studies also demonstrated that the stronger the magnetic field applied, the higher the drug release from the deformed PDMS sponge cylinder and thus more obvious inhibition effects on Trex cell growth. All results confirmed that the device can provide a safe, long-term, triggerable and reutilizable way for localized disease treatment such as cancer.

Keywords: 3D printing; fused deposition modelling; FDM; magnetic field; polydimethylsiloxane sponge; triggerable drug delivery system; carbonyl iron; iron oxide; 5-fluorouracil; personalized medicine

1. Introduction

The objective of drug delivery systems is to provide predetermined drug release profiles ensuring optimal distribution and absorption of pharmaceutical compounds, which enhance therapeutic effectiveness and minimize side effects by offering a safer, more convenient, and efficient drug administration in humans with enhanced patient compliance [1][2]. Predetermined drug release profiles could be achieved by optimizing suitable drug delivery systems (DDSs) as such enhanced efficacy, safety, and patient compliance may be realized through optimal drug distribution and absorption in the targeted location at the (sub)cellular level [2][3]. However, it has been difficult for conventional drug delivery system to maintain drug concentration level within the narrow therapeutic concentration window for avoiding ineffectiveness (underdose) or toxicity (overdose), and it is often impossible to modify the drug release from these systems after administration [1][4][5]. Additionally, it may not always be appropriate for untunable monotonic drug release to be applied in some disease treatments which require variable release kinetics (including cancer, diabetes, pain, and myocardial infarction) [1][4]. Also, drugs are needed to be administered multiple times or continuously for achieving a long-acting drug release profile in some circumstances [4]. This may lead to patients' discomfort or inconvenience and even the addition of external devices. Therefore, it is important to design a drug delivery system, which can modulate drug release in terms of time, rate, and location. Such a drug delivery system would show considerable advances in delivering drugs, like painkillers, hormones, and chemotherapeutic agents [1].

Triggerable drug delivery systems (TDDSs), capable of releasing drug through applying external physical signals (such as magnetic field, ultrasound, pH, enzymes, temperature, electric, light, and near-infrared radiation) are gaining more and more attention in

pharmaceutical sciences [1][6][7]. Such systems containing a large amount of drug can present remote, noninvasive, tunable, and reliable switching of therapeutic compound flux [4]. Hence, spatiotemporal management of drug availability could be realized through these triggerable drug delivery systems by the physicians or patients with the utilization of either the interaction between a 'responsive' material and the surrounding environment or a remotely controllable activation device [1][5][8]. Also, these systems loaded with a large amount of drug can achieve multiple dosing after a single administration through repeatable triggering [1]. However, there are still some limitations, like low controllability because of an initial burst release or a drug leakage via diffusion, difficulty in disposing of the systems after therapy, and increasing toxicity-associated risks due to the possible degradation of the matrix and the reduction of stability and reliability of the systems [1][5].

Implantable reservoir-based devices have been designed to overcome these limitations efficiently [9]. Targeted therapy could be achieved through these devices at different length scales with high anatomical variability [10]. The performing procedure and working environment will affect the features, sizes, and operation mechanisms significantly [5]. Herein, it is highly desirable to fabricate untethered macroscale triggerable drug delivery systems with low cost, simple preparation, facile operation, simplified structural morphology, and the ability to move through body channels and perform on-demand drug administration [5][11].

Although several external stimuli have been studied in TDDSs, controlled drug targeting through magnetic actuation is still one of the principal approaches because of many advantages, such as instantaneous and reversible response, remote actuation, non-destructive and high controllability, which are especially attractive for biomedical fabrication where the noncontact feature is particularly necessary *in vivo* environment with absolute safety [3][12][13]. Those magnetic systems also play an important role in cancer research due to the superior ability in chemotherapy by realizing: (1) selective delivery of the maximum fraction of anti-cancer molecules to the desired site without any increase in side effects to normal cell; (2) prior distribution of anti-cancer drug to targeted cells; (3) stable systemic drug concentration and (4) elimination of normal tissue clearance with the application of external magnetic field [3]. Various types of magnetic particles have been widely applied in these systems as switching

carriers, including Fe_3O_4 particles [7][14], NdFeB powders [5] and carbonyl iron (CI) powders [12][13]. With the addition of magnetic enclosures, these magnetically responsive systems can move and deform due to applied magnetic fields [15]. Furthermore, with the manipulation of external permanent magnets, magnetic triggering drug delivery systems have the ability to remote locomotion through biological tissues in real-time because magnetic fields can transmit high force or torques wirelessly with multiple degrees of freedom to medical robots [5][16].

In recent years, personalized medicine has attracted increasing attention as it can provide patients with a superior treatment with a comprehensive consideration of their own pharmacogenomics, anatomical, and physical conditions [17]. It is reported that the inappropriate dosing or dosing combination has become the main reason for adverse effects from drug therapy [18]. This leads to an increased demand for a tailored method of dosage forms to suit patient needs instead of "One-size-fits-all" [18][19].

To address these challenges, three-dimensional printing (3DP) technology has been applied successfully because traditional DDSs cannot fulfil such criteria [17][19]. Because of its potential in personalized medicine, its applications in medical devices, implants, tissue engineering, and pharmaceutical dosage forms have attracted a great deal of attention [18]. This technology can achieve detailed and flexible spatial composition, and provide more available starting materials (like colloidal inks, bio-inks, and polymers) for the unprecedented complex and precise manufacture of 3D DDSs [2][20]. Various techniques, namely powder-based (PB), stereolithography (SLA), selective laser sintering (SLS), inkjet printing and fused deposition modelling (FDM) have been explored in the pharmaceutical applications [19]. Among them, FDM 3DP has gained the most attention due to its cost-effective, time-saving and versatile modalities of producing sophisticated solid objects [18][19].

Polylactic acid (PLA) is the most common material used for FDM because it is a non-toxic, renewable, thermoplastic, biodegradable and biocompatible polymer [20][21]. Additionally, its suitable properties like high mechanical strength, low coefficient of thermal expansion and processability for extrusion applications make this material ideal for pharmaceutical and biomedical applications [21]. Furthermore, various polymers, such as Pluronic, poly(vinyl alcohol) and polycaprolactone, could be blended with PLA to provide extra features with the

addition of active pharmaceutical ingredients (APIs) to the final composite material in healthcare applications [20][21][22][23].

In this study, a magnetic-field triggerable drug delivery system with a 3D-printed reservoir and magnetic PDMS sponges was designed and characterized. This device can achieve highly precise and dynamic administration of drugs in an active and instant manner with only a permanent magnet.

2. Materials and Methods

2.1. Materials

A SYLGARD® 184 Silicone Elastomer prepolymer (Sylgard 184A, $M_w \approx 22\,000$ g·mol^{-1}) and the thermal curing agent (Sylgard 184B, $M_w \approx 15\,000$ g·mol^{-1}) were purchased from Dow Corning. Carbonyl iron (CI) powder with purity ≥ 97% was purchased from Sigma-Aldrich (Germany). The white granulated sugar was purchased from Sainsbury's (UK). The model anticancer drug 5-fluorouracil (FLU) with purity > 98% was purchased from Hangzhou Longshine Bio-tech Co., Ltd. (Hangzhou, China). The PLA filament (FilaPrint® premium PLA, 1.75 mm) was purchased from 3D FilaPrint Ltd. (Essex, UK). All chemicals used were of analytical or food grade and used as received.

2.2. Preparation of PDMS Sponges

An eco-friendly sugar templating method was applied to fabricate porous magnetic sponges in this study because the commercially available household sugar which is used as the mould could be removed easily through immersion in water afterwards [24]. Around 15 g sugar was thoroughly mixed with 0.5 mL water and pressed firmly in a Petri dish (diameter = 5 cm). Then the Petri dish was placed in a convection oven (Memmert, UF110, Schwabach, Germany) at 50°C for around 1 h to dry the sugar for achieving a mould of connected sugar particles [1]. PDMS prepolymers and curing agents were mixed by a weight ratio of 10:1. Then the magnetic microparticles were blended with the well-mixed PDMS solution at different magnetic particle:PDMS weight ratios of 0:10 (0 w/w %), 3:10 (30 w/w %), 5:10 (50 w/w %), 10:10 (100 w/w %) or 15:10 (150 w/w %). After that, the mixture was poured onto the dried sugar

mould and then the mixture was infiltrated into the sugar template because of capillary force [24]. The Petri dish was placed in the oven again at 70°C for 3 h for the curing process. Finally, the cured blend was immersed in water to dissolve the sugar completely. After the removal of the sugar templates, 3D eco-friendly interconnected microporous PDMS sponges were formed.

2.3. Preparation and Characterization of the Reservoir

2.3.1. Design of the Reservoir

The model reservoir was designed using Solidworks (2017 SP5, Waltham, MA, USA) and converted to a stereolithography file (.stl). For the ease of printing operation, the geometry of the 3D printed reservoirs was selected as cylinder shape because of the large surface area in contact with the building plate [25]. The currently optimized design was flat cylindrical with a smoothed edge and consisting of two parts: top and bottom (Figure 1 A and B). The diameter and height of the reservoir are 19 mm and 7 mm respectively. The diameter and height of the hollow space for sponges are 12.5 mm and 5 mm respectively. In addition, there is a small aperture (diameter = 1.5 mm) at the centre of the top part surface.

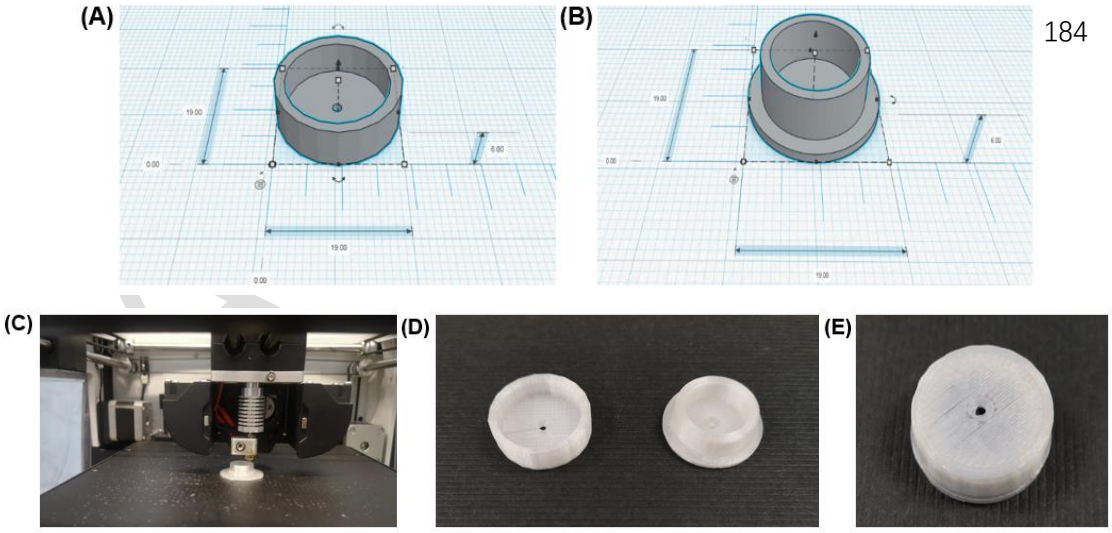

	weight (g)	diameter (mm)	height (mm)
top part	0.811±0.003	19.367±0.045	6.153±0.069
bottom part	0.980±0.005	19.385±0.029	6.662±0.050
whole reservoir	1.791±0.007	19.385±0.029	7.764±0.061

Figure 1. Stereolithography images of (A) the bottom part and (B) the top part of the reservoir. (C) The printing process of the PLA reservoir with Robo R2. (D) Macroscopic appearance of 3D-printed PLA reservoir (left: bottom, right: top). (E) Macroscopic appearance of the

assembled 3D-printed PLA reservoir loaded with 100% CI/PDMS sponge and drug solution. Dimensions and weight of the 3D printed reservoir are also shown (n = 6). The dimention and weight of each part was also added in this figure.

2.3.2. FDM 3DP of the Reservoir

Printing was performed in a Robo R2 (San Diego, CA, USA) using a nozzle with a diameter of 0.4 mm for printing PLA 1.75 mm 3D printer filaments. The following settings were employed: the printing temperature (T_{print}) was set at 195 °C, $T_{platform}$ = 60 °C, infill pattern = light, layer height = 0.1 mm.

2.3.3. Appearance, dimensions, and microstructure of the reservoir

Samples prepared by FDM were photographed and were visually investigated. The diameter and height of the 3D printed reservoirs were measured with a vernier calliper. The radial expansion coefficient (E_r) of filaments was calculated according to Eq. 1, where D_f and D_0 represent the diameters of filament and die of printer respectively [26].

$$E_r(\%) = \frac{D_f}{D_0} \times 100\% \quad \text{(Eq. 1)}$$

The printed reservoir (top and bottom part) was examined by Jeol JMS 820 scanning electron microscopy (Freising, Munich, Germany) at the accelerating voltage of 3 kV. The samples were mounted on an aluminium stub using adhesive carbon tape and were sputter-coated with gold under vacuum (Edwards S-150 sputter coater, Edwards High Vacuum Co. International, Albany, NY, USA).

2.4. Assemble and Drug Loading of the TDDS

2.4.1. Preparation of Drug Solution

The model drug in this study, 5-fluorouracil (FLU), is sparingly soluble in water and slightly soluble in ethanol [27], so it is necessary to design how to increase the dose of FLU loaded into the device. However, the solubility of 5-fluorouracil can be affected significantly by temperature as it can increase more than 12-fold by enhancing the temperature between 25 and 200°C under the constant pressure of 5.1 MPa [28]. Additionally, Singh et al. point out that 5-fluorouracil has good thermal stability when the temperature is less than 278°C [29]. Therefore,

the temperature of the solution was increased in the preparing process.

2.4.2. Device Integration and Assembly

The sponge cylinders which can fit the shape of the hollow space of the reservoir bottom will be cut and then immersed into the drug solution. After the sponge cylinder absorbed enough drug solution, it was taken out and placed into the bottom hollow. Then the two parts of the reservoir were closed tightly.

2.4.3. Drug Loading of the Device

By comparing the weight change of the device before and after the drug loading process, the amount of drug loaded into the device could be calculated every time afterwards because the weight ratio of the drug to the solution is constant.

2.5. Dissolution Test under Sink Conditions

In vitro dissolution tests under sink conditions were performed with a US Pharmacopeia (USP) type I basket or type II paddle apparatus (708-DS Dissolution Apparatus, Agilent Technologies, USA) in 900 mL of PBS (pH 6.8) at 37 ± 0.3 °C with the paddle speed of 100 rpm according to different designed modes (Figure 2). The drug concentration in the dissolution medium was measured automatically using Cary 60 UV-Vis (Agilent Technologies, USA) at a wavelength of 265 nm in a 1 cm cell versus a blank solution consisting of PBS (pH 6.8). All samples were run in triplicate (n = 3). Then the release profile could be plotted as a percentage of cumulative drug release versus time. The preliminary results showed that the materials used in 3D printing such as PLA does not interfere with drug detection and UV absorbance. The standard curve was prepared in the concentration of 0.625-20 μg/mL ($A = 0.0514C + 0.002$, R^2=0.9995) where A is the absorbance and C is the concentration (μg/ml).

To study the effect of the position of magnet versus device containing the sponge, various modes were employed. In Mode 1 (Figure 2A), the device was lying on the magnet. In Mode 2 (Figure 2B), there is no magnet. In Mode 3 (Figure 2C), the device was standing on the

magnet. In Mode 4 (Figure 2D), the device was placed in the basket without magnet.

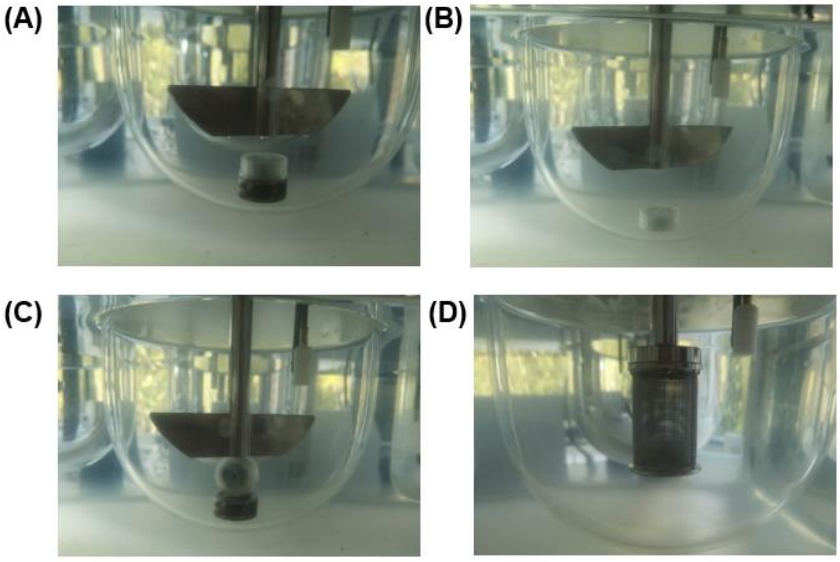

Figure 2. Various modes for comparing the drug release from the device. (A) Mode 1: the device was laid flat on the magnet; (B) Mode 2: the device with no magnets; (C) Mode 3: the device was placed vertically on the magnet; (D) Mode 4: the device was placed in the basket without magnets.

Neodymium grade N42 magnets were applied for providing different magnetic flux densities with a distance of 5 mm for the device during the dissolution testing (Table 1).

Table 1. Dimensions of magnets used in the current studies to provide different magnetic flux densities with 5 mm distance between the specimen and magnets

Magnets	A*	B	C	D
diameter (mm)	19.5	19.5	21.5	19.5
thickness (mm)	2.5	2.5	5.5	9.5
magnetic field (mT)	110	150	204	355

*The effect of this magnet was not further investigated as it did not show a significant deformation on sponges

The similarity factor (f_2) in Eq. 2 was developed by Moore and Flanner as a model-independent mathematical method to analyze the closeness among these dissolution profiles [30]:

$$f_2 = 50 \times \log\{[1 + \frac{1}{n}\sum_{t=1}^{n}(R_t - T_t)^2]^{-0.5} \times 100\} \quad \text{(Eq. 2)}$$

where n is the number of dissolution time points, R_t and T_t are the dissolution value of the reference and test sample at the time t, respectively.

The mathematical method of f_2 has been adopted by many guidance, like Food and Drug Administration (FDA) and European Medicines Agency (EMEA), as a criterion for measurement of the similarity between in vitro dissolution profiles [31]. As the value of f_2 equals to 100 when the two profiles are identical and the value is 50 when an average variation of 10% at all determined time points, a public standard for f_2 value between 50 and 100 can indicate the two dissolution profiles are similar, whereas the value of less than 50 can show the two profiles are different.

2.6. Cell Studies of the Devices in Vitro with FLU Solution

2.6.1. Preparation of Sponges Samples Loaded with Drug Solution

As the sponge samples are very porous, it is easy for the drug solution penetrates the sponge and retained by the sponge. Three samples of each sponge formulation (diameter × thickness = 5 mm × 2 mm) were compressed gently in the drug solution until no air bubbles come out. After that, the sponge samples with drug solutions were taken out and leave them at room temperature.

2.6.2. Cell Lines

HeLa and Trex cells both stably express green fluorescent protein (GFP) constructs. Cell lines were maintained in Dulbecco's modified Eagle medium (DMEM) supplemented with 10% fetal calf serum (FCS), penicillin/streptomycin and L-Glutamine at 37°C and 5% CO_2.

2.6.3. Experimental Set-Up

Substrates transferred to 12 well plates and sterilized with UV irradiation 30 min prior to adding cells. Cells were plated at a density of 0.4×10^5 on day 0. Day 1, substrates were transferred to new wells to avoid any effect of cell dissociation. Cells remaining cells were trypsinized using trypsin EDTA and counted using a hemocytometer to determine cell number. Cells were re-

plated onto the transferred substrates in fresh media. Day 4, substrates were removed and discarded and remaining cells trypsinized, counted and discarded as before. Images were taken prior to trypsinisation.

3. Results and Discussion

3.1. Fabrication and Characterization of Magnetic PDMS Sponges

Among all prepared magnetic PDMS sponges (Figure 3), 100 w/w% CI/PDMS sponge was selected for the scaffold in this experiment as it exhibited the most deformation tendency at the given reflux under certain magnetic fields. The underlying reasons being that the ferromagnetic particles were homogeneously distributed throughout the PDMS sponges as such it was enough to deform the sponges at a suitable extent to trigger drug release from the system. The lower or higher amount of CI particles in the formulation exhibited insufficient or excessive reflux in the experimental set-up, respectively. Based on the preliminary results, 100% w/w CI/PDMS formulation was selected for the additional studies.

Figure 3. Photograph of the pure PDMS sponge cylinder, CI loaded PDMS cylinder and cube.

3.2. Fabrication and Characterization of the Reservoir

3.2.1. Printing the Device

The PLA filaments were transformed into reservoirs via a Robo R2 FDM 3D printer (Figure 1C). The suitable size of the sponge cylinder was cut and subsequently installed into the PLA reservoir bottom before the top part assembling and drug loading. The reservoir could be opened later, meanwhile, both the reservoir and PDMS sponge cylinders could be washed completely and reutilized (Figure 1B). These printed reservoirs showed satisfactory mechanical properties. These two parts of the reservoir are white, non-friable, plastic-like and can be closed tightly. The printed reservoirs show low variability in both size and weight (Figure 1).

3.2.2. Characterization of 3D Printed Reservoirs

The extruded PLA filament was smooth and uniform with a diameter of 0.403±0.001 mm. The value of E_r (100.75 %) reduced the possibility of die swelling, which may cause uneven filament blocking the feed nozzle (ø=0.4 mm) of the printer. SEM analysis (Figure 4) confirmed that the printed reservoir has a layered structure as the printing was conducted in a layer-by-layer manner.

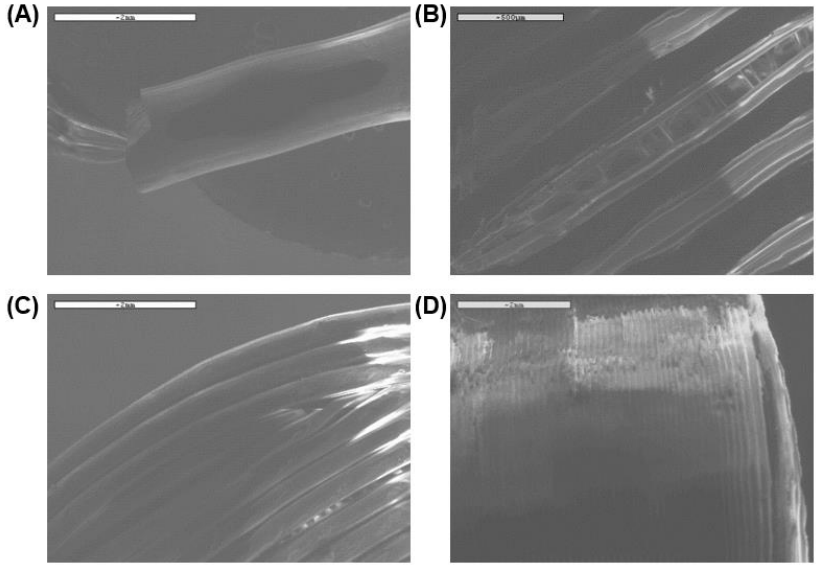

Figure 4. SEM images of (A) PLA filaments, (B) the bottom surface of the reservoir, (C) the top surface of the reservoir, (D) the side surface of the reservoir.

3.3. Assemble and Drug Loading of the TDDS

The sponge cylinders with the diameter and height of 12.5 mm and 5mm respectively were cut carefully and loaded into the hollow space of the reservoir bottom. Then the two parts of the reservoir can be closed tightly (Figure 1E).

After the pure PDMS sponge or the CI-loaded PDMS sponge was assembled into the reservoir, around 0.3 mL solution could be loaded into the device because of the strong water absorption of the sponge samples. The dose of drug loaded into the device could be calculated by analyzing the weight change (weight of solution) of the device before and after the drug loading process. The maximum concentration of the FLU solution was optimized at 25 mg/mL [27]. As a result, the device containing around 7~8 mg FLU was assembled successfully.

3.4. *Dissolution Test under Sink Conditions*

It is assumed that the location of magnetic bar respect to the location of the reservoir containing sponge can deform sponge differently and this, in turn, releases the drug with the different pattern when compared to the release behaviour of the device without magnets (Figure 5). Some drug solutions can release from the small aperture gradually without magnets (Mode 2). When the magnet bar is contacted with the side part of the device, the magnetic sponge loaded with the drug solution can move close to the magnetic bar because of the magnetic field and drug solution is squeezed out through the small aperture (Mode 3). In contrast, the magnetic sponge and drug solution moves away from the aperture when the magnetic bar is at the bottom of the device, so only a little amount of drug solution will be released (Mode 1). To prove this hypothesis, dissolution tests under sink conditions were carried out.

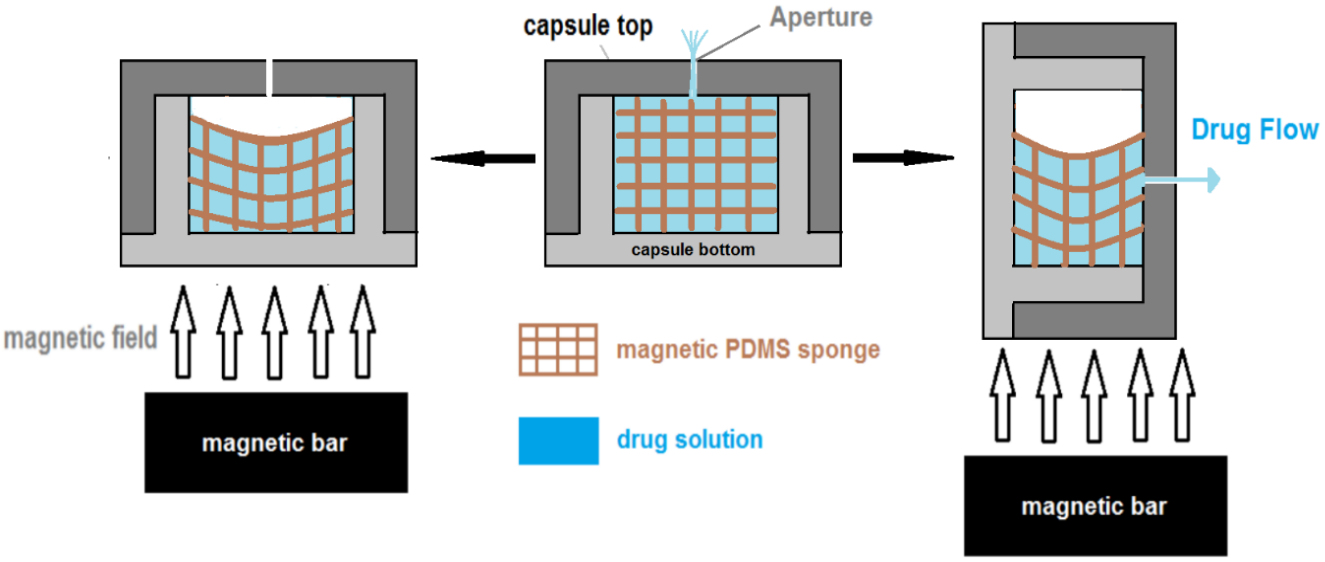

Figure 5. A schematic cross-section view diagram showing the release mechanism of the device with the utilization of the magnetic field from different directions (left: Mode 1, middle: Mode 2, right: Mode 3).

In vitro drug release profiles from the same drug-loaded device but with different utilizations of magnets are depicted in Figure 6. The dissolution test was carried out for 12 h, and the results showed that over 80% of the drug released in Model 3 within the first 720 min.

When the device was standing on Magnet D (Model 1), the dissolution rate was faster than other models. The probable reasons may have been the drug solution could release from the small aperture because of the deformation caused by the magnetic field. In particular, the time at which 10%, 50%, 80% and 90% of the drug were dissolved ($T_{10\%}$, $T_{50\%}$, $T_{80\%}$ and $T_{90\%}$ respectively) are observed at <5, 20, 55 and 140 min (Figure 6). When Model 7 which the device was standing on Magnet B (the smaller magnetic field) and compared with Model 1 (the stronger magnetic field), the drug release was much faster from Model 1 (f_2 =40.58) mainly due to the more obvious deformation caused by a stronger magnetic field.

However, the drug release from the device which was lying on the magnet (Model 5) is dramatically slow. The comparison of dissolution profiles of Model 1 with model 5 demonstrated that the deformation of the magnetic sponge in Model 1 is more efficient than Model 5 because of the position of the small aperture and the size differences between the diameter and height of the sponge samples assembled in the reservoir (f_2 =9.71).

Besides, there are also significant differences between Models 1 and 2 (f_2 =30.03), Models 2 and 5 (f_2 =15.66). This indicates that the different utilizations of the external magnetic field have crucial influences on the dissolution behaviour of drug release from the device. The dissolution behaviours of the drug-loaded device are different in basket and paddle methods because of the obvious difference between Model 2 and 3 (f_2 =30.03), Model 4 and 5 (f_2 =50.56).

To prove the small aperture on the top of the reservoir is the main pathway for drug-releasing, the device without any aperture was designed, fabricated and analyzed (Model 6) in the same way as Model 2. During the 12 h, only 16% of drug loading was released from the device and

the amount is much lower than that of Model 2. This indicates that the drug solution is mainly released from the small aperture. However, the slower drug release in Model 8 when compared with Model 5 indicates that the weaker magnetic field can release less drug in Mode 1.

It can be concluded that the switching "on" state in the release pattern from the device can be triggered when the magnet is employed like Model 1, and the switching "off" drug-releasing of the device can also be realized when we change the position of the magnets like Model 8. Consequently, the release of drugs from this device can be controlled repeatedly and quickly. All these features make this novel implantable drug delivery device a promising candidate to tailor and control the release of therapeutic substances in local disease therapy. The device could be navigated to the target site *in vivo* wirelessly with the application of magnetic fields. With the development of this TDDS, the anticancer agent (FLU) could be navigated to the target site and released at an adjustable rate in accordance with patients' specific conditions for minimizing adverse effects during cancer treatment. Herein, the bioavailability of FLU could be enhanced significantly. Furthermore, this device shows superior potential in hormone deficiencies and chronic pain treatments. Desirable doses of these drugs, like hormones and painkillers, can be released by loading these drug solutions of various concentrations into the drug delivery system.

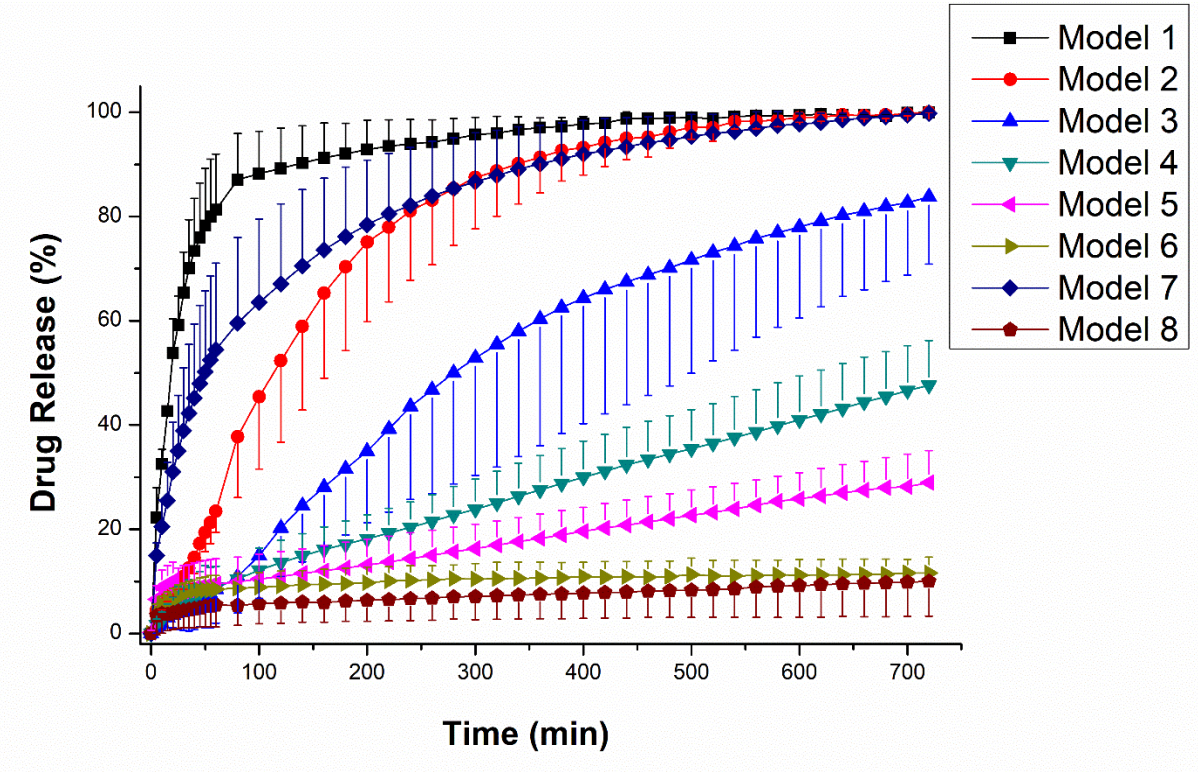

Model	Basket/Paddle	Magnet	Mode	Aperture	$T_{10\%}$	$T_{50\%}$	$T_{80\%}$	$T_{90\%}$
1	Paddle	D	3	√	<5 min	20 min	55 min	120 min
2	Paddle	×	2	√	25 min	120 min	240 min	340 min
3	Basket	×	4	√	80 min	280 min	640 min	-
4	Basket	D	1	√	80 min	-*	-*	-
5	Paddle	D	1	√	80 min	-*	-	-
6	Paddle	×	2	×	220 min	-*	-	-
7	Paddle	B	3	√	<5 min	50 min	220 min	360 min
8	Paddle	B	1	√	720 min	-	-	-

Figure 6. *In vitro* mean drug release profiles (±SD) (under sink condition) in PBS (pH 6.8) of device loaded with 25 mg/mL FLU solution (n = 3). Different models and the time at which 10%, 50%, 80% and 90% of the drug were dissolved are clarified underneath the dissolution profiles for the comparison of drug release behaviours of the device.

3.5. Cell Studies *in vitro*

It is necessary to analyze the cell inhibition behaviour of FLU loaded 3D printed reservoir and sponge samples. The assessment of cell numbers of Trex cells was designed as follows. The cell numbers in Figure 7 (Group B1, B9 with B11, Group B2 with B10) display that these PDMS sponges, especially CI loaded PDMS sponge without the drug can inhibit the growth of

Trex cells to some extent, but the number of Trex cells still increased within 4 days because there are no FLU solution. Through comparing data of groups under the same conditions just except for applying magnetic fields (Group B9 with B10, Group B1 with B2, and Group B3 with B4), it can be concluded that stronger magnet will lead to more drugs being released from the deformation of magnetic sponges and more obvious inhibition effects on Trex cell growth. Importantly, sponge samples loaded with a higher concentration of FLU solution (Group B3 with B5, Group B4 with B6) present a stronger inhibition effect on Trex cells. The results showed that there is no difference between Group 7 and 8 and this is not surprising because the magnet would not trigger the release of drug solution loaded in the device when the magnets were placed at the bottom of the whole device as reflected by the results highlighted in the dissolution section.

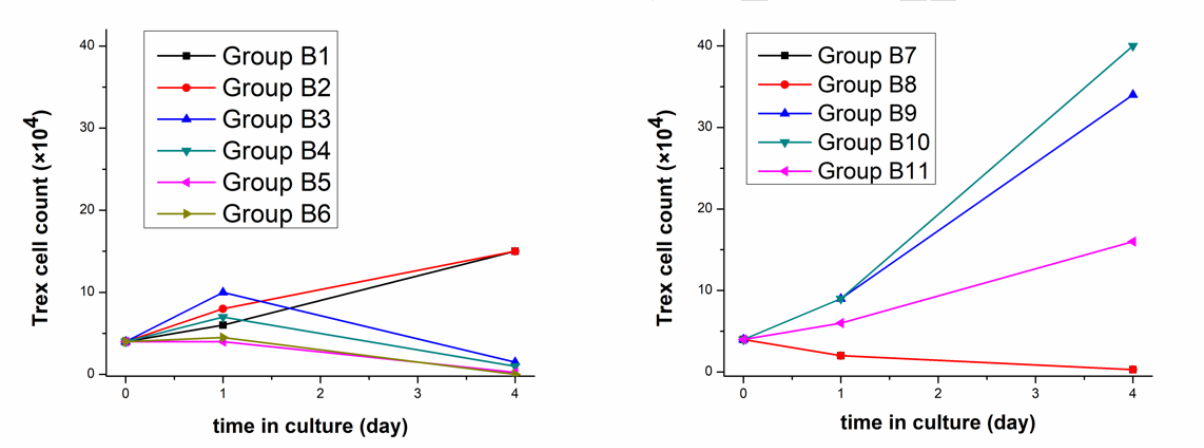

Group	Magnet	Sponge	FLU Solution	PLA Reservoir
B1	B	CI/PDMS=100 wt%	×	×
B2	C	CI/PDMS=100 wt%	×	×
B3	B	CI/PDMS=100 wt%	12.5 mg/mL	×
B4	C	CI/PDMS=100 wt%	12.5 mg/mL	×
B5	B	CI/PDMS=100 wt%	25 mg/mL	×
B6	C	CI/PDMS=100 wt%	25 mg/mL	×
B7	×	CI/PDMS=100 wt%	12.5 mg/mL	√
B8	B	CI/PDMS=100 wt%	12.5 mg/mL	√
B9	B	×	×	×
B10	C	×	×	×
B11	B	pure PDMS	×	×

Figure 7. Numbers of Trex cells under different conditions. 3D printed PLA reservoir and sponge samples loaded with different solutions under different magnetic fields (for better

clarification the composition for each group was added in the table attached to the figure).

In summary, stronger magnetic fields can lead to larger deformations of CI-loaded PDMS sponge cylinders and a higher volume of drug solution will be released from the drug-loaded magnetic PDMS sponges. By adjusting the concentration of the drug solution, the dose of the drug could be changed. Because the prepared magnetic sponge sample can release a specific volume of drug solution under the same magnetic field, the lower loaded solution concentration can lead to the lower loaded dose of the drug. With the assembly of a 3D printed PLA reservoir, there will be no obvious difference of released dose of drug from the whole device between the device having magnets placed underneath and the device alone without magnets.

Conclusion

In this experiment, we designed and developed a novel implantable drug delivery device assembled from a magnetic PDMS sponge cylinder and a 3D-printed PLA reservoir to provide a triggerable and remotely controllable system for on-demand drug delivery in localized disease treatment. This device utilizes different extrinsic magnetic fields for offering a tunable force to trigger drug release through reversible magnetic sponge deformations. The geometric shape and dimensions of the reservoir could be adjusted easily through FDM 3D printing technology according to the requirement of patients. In addition, the drug-releasing dose and timing can be reliably and flexibly controlled by different applications of the magnetic field to fit the prescribed needs. Furthermore, this device has the potential to be optimized as a safe and long-term implant because of its large drug loading ability. It can be the key component of a multi-functional, implantable and smart drug delivery system for the controlled release of therapeutic substances to avoid frequent injection or various sophisticated dosing regimens. In the future, combining the device with *i.e.* sensing system can also offer protection for biosensors because biofouling and exposure to the body may lead to the failure of biosensors *in vivo*.

Acknowledgement

The authors thanks China Scholarship Council (CSC) for financial support of Kejing Shi.

Conflict of Interest

The authors declare no conflict of interest

References

[1] A. Shademani, H. Zhang, J.K. Jackson, M. Chiao, Active Regulation of On-Demand Drug Delivery by Magnetically Triggerable Microspouters, Adv. Funct. Mater. 27 (2017). https://doi.org/10.1002/adfm.201604558.

[2] S.E. Moulton, G.G. Wallace, 3-dimensional (3D) fabricated polymer based drug delivery systems, J. Control. Release. 193 (2014) 27–34. https://doi.org/10.1016/j.jconrel.2014.07.005.

[3] J.L. Arias, V. Gallardo, F. Linares-Molinero, A. V. Delgado, Preparation and characterization of carbonyl iron/poly(butylcyanoacrylate) core/shell nanoparticles, J. Colloid Interface Sci. 299 (2006) 599–607. https://doi.org/10.1016/j.jcis.2006.03.005.

[4] B.P. Timko, T. Dvir, D.S. Kohane, Remotely triggerable drug delivery systems, Adv. Mater. 22 (2010) 4925–4943. https://doi.org/10.1002/adma.201002072.

[5] V. Iacovacci, G. Lucarini, L. Ricotti, P. Dario, P.E. Dupont, A. Menciassi, Untethered magnetic millirobot for targeted drug delivery, Biomed. Microdevices. 17 (2015). https://doi.org/10.1007/s10544-015-9962-9.

[6] M. Sitti, H. Ceylan, W. Hu, J. Giltinan, M. Turan, S. Yim, E. Diller, Biomedical Applications of Untethered Mobile Milli/Microrobots, Proc. IEEE. 103 (2015) 205–224. https://doi.org/10.1109/JPROC.2014.2385105.

[7] X. Zhao, J. Kim, C.A. Cezar, N. Huebsch, K. Lee, K. Bouhadir, D.J. Mooney, Active scaffolds for on-demand drug and cell delivery, Proc. Natl. Acad. Sci. 108 (2011) 67–72. https://doi.org/10.1073/pnas.1007862108.

[8] A.Y. Rwei, J.L. Paris, B. Wang, W. Wang, C.D. Axon, M. Vallet-Regí, R. Langer, D.S. Kohane, Ultrasound-triggered local anaesthesia, Nat. Biomed. Eng. 1 (2017) 644–653. https://doi.org/10.1038/s41551-017-0117-6.

[9] J.M. Maloney, S.A. Uhland, B.F. Polito, N.F. Sheppard, C.M. Pelta, J.T. Santini, Electrothermally activated microchips for implantable drug delivery and biosensing, J. Control. Release. 109 (2005) 244–255. https://doi.org/10.1016/j.jconrel.2005.09.035.

[10] W. Kempin, C. Franz, L.C. Koster, F. Schneider, M. Bogdahn, W. Weitschies, A. Seidlitz, Assessment of different polymers and drug loads for fused deposition modeling of drug loaded implants, Eur. J. Pharm. Biopharm. 115 (2017) 84–93. https://doi.org/10.1016/j.ejpb.2017.02.014.

[11] S.A. Stewart, J. Domínguez-Robles, V.J. McIlorum, E. Mancuso, D.A. Lamprou, R.F. Donnelly, E. Larrañeta, Development of a biodegradable subcutaneous implant for prolonged drug delivery using 3D printing, Pharmaceutics. 12 (2020). https://doi.org/10.3390/pharmaceutics12020105.

[12] S. Jiang, Y. Hu, H. Wu, Y. Zhang, Y. Zhang, Y. Wang, Y. Zhang, W. Zhu, J. Li, D.

Wu, J. Chu, Multifunctional Janus Microplates Arrays Actuated by Magnetic Fields for Water/Light Switches and Bio-Inspired Assimilatory Coloration, Adv. Mater. 31 (2019) 1–8. https://doi.org/10.1002/adma.201807507.
[13] J.H. Kim, S.M. Kang, B.J. Lee, H. Ko, W.G. Bae, K.Y. Suh, M.K. Kwak, H.E. Jeong, Remote Manipulation of Droplets on a Flexible Magnetically Responsive Film, Sci. Rep. 5 (2015) 1–10. https://doi.org/10.1038/srep17843.
[14] K. Cai, Z. Luo, Y. Hu, X. Chen, Y. Liao, L. Yang, L. Deng, Magnetically triggered reversible controlled drug delivery from microfabricated polymeric multireservoir devices, Adv. Mater. 21 (2009) 4045–4049. https://doi.org/10.1002/adma.200900593.
[15] X. Hu, G. Nian, X. Liang, L. Wu, T. Yin, H. Lu, S. Qu, W. Yang, Adhesive Tough Magnetic Hydrogels with High Fe 3 O 4 Content, ACS Appl. Mater. Interfaces. 11 (2019) 10292–10300. https://doi.org/10.1021/acsami.8b20937.
[16] F. Munoz, G. Alici, H. Zhou, W. Li, M. Sitti, Analysis of Magnetic Interaction in Remotely Controlled Magnetic Devices and its Application to a Capsule Robot for Drug Delivery, IEEE/ASME Trans. Mechatronics. 23 (2018) 298–310. https://doi.org/10.1109/TMECH.2017.2764902.
[17] K. Pietrzak, A. Isreb, M.A. Alhnan, A flexible-dose dispenser for immediate and extended release 3D printed tablets, Eur. J. Pharm. Biopharm. 96 (2015) 380–387. https://doi.org/10.1016/j.ejpb.2015.07.027.
[18] M.A. Alhnan, T.C. Okwuosa, M. Sadia, K.W. Wan, W. Ahmed, B. Arafat, Emergence of 3D Printed Dosage Forms: Opportunities and Challenges, Pharm. Res. 33 (2016) 1817–1832. https://doi.org/10.1007/s11095-016-1933-1.
[19] C.I. Gioumouxouzis, A.-T. Chatzitaki, C. Karavasili, O.L. Katsamenis, D. Tzetzis, E. Mystiridou, N. Bouropoulos, D.G. Fatouros, Controlled Release of 5-Fluorouracil from Alginate Beads Encapsulated in 3D Printed pH-Responsive Solid Dosage Forms, AAPS PharmSciTech. 19 (2018) 3362–3375. https://doi.org/10.1208/s12249-018-1084-2.
[20] K. Liang, S. Carmone, D. Brambilla, J.-C. Leroux, 3D printing of a wearable personalized oral delivery device: A first-in-human study, Sci. Adv. 4 (2018) eaat2544. http://advances.sciencemag.org/.
[21] J. Domínguez-Robles, N. Martin, M. Fong, S. Stewart, N. Irwin, M. Rial-Hermida, R. Donnelly, E. Larrañeta, Antioxidant PLA Composites Containing Lignin for 3D Printing Applications: A Potential Material for Healthcare Applications, Pharmaceutics. 11 (2019) 165. https://doi.org/10.3390/pharmaceutics11040165.
[22] J. Fu, X. Yu, Y. Jin, 3D printing of vaginal rings with personalized shapes for controlled release of progesterone, Int. J. Pharm. 539 (2018) 75–82. https://doi.org/10.1016/j.ijpharm.2018.01.036.
[23] D. Li, G. Guo, R. Fan, J. Liang, X. Deng, F. Luo, Z. Qian, PLA/F68/Dexamethasone implants prepared by hot-melt extrusion for controlled release of anti-inflammatory drug to implantable medical devices: I. Preparation, characterization and hydrolytic degradation study, Int. J. Pharm. 441 (2013) 365–372. https://doi.org/10.1016/j.ijpharm.2012.11.019.
[24] S.J. Choi, T.H. Kwon, H. Im, D. Il Moon, D.J. Baek, M.L. Seol, J.P. Duarte, Y.K. Choi, A polydimethylsiloxane (PDMS) sponge for the selective absorption of oil from

water, ACS Appl. Mater. Interfaces. 3 (2011) 4552–4556. https://doi.org/10.1021/am201352w.
[25] Q. Li, H. Wen, D. Jia, X. Guan, H. Pan, Y. Yang, S. Yu, Z. Zhu, R. Xiang, W. Pan, Preparation and investigation of controlled-release glipizide novel oral device with three-dimensional printing, Int. J. Pharm. 525 (2017) 5–11. https://doi.org/10.1016/j.ijpharm.2017.03.066.
[26] Y. Yang, H. Wang, H. Li, Z. Ou, G. Yang, 3D printed tablets with internal scaffold structure using ethyl cellulose to achieve sustained ibuprofen release, Eur. J. Pharm. Sci. 115 (2018) 11–18. https://doi.org/10.1016/j.ejps.2018.01.005.
[27] K. Shi, D. Tan, A. Nokhodchi, M. Maniruzzaman, Drop-On-Powder 3D Printing of Tablets with an Anti-Cancer Drug, 5-Fluorouracil, Pharmaceutics. 11 (2019) 150. https://doi.org/10.3390/pharmaceutics11040150.
[28] S. Akay, B. Kayan, Y. Yang, Solubility and Chromatographic Separation of 5-Fluorouracil under Subcritical Water Conditions, J. Chem. Eng. Data. 62 (2017) 1538–1543. https://doi.org/10.1021/acs.jced.7b00015.
[29] P. Singh, G. Tyagi, R. Mehrotra, A.K. Bakhshi., Thermal stability studies of 5-fluorouracil using diffuse reflectance infrared spectroscopy, Drug Test. Anal. 1 (2009) 240–44. https://doi.org/10.1002/dta.41.
[30] J.W. Moore, H.H. Flanner, Mathematical Comparison of Dissolution Profiles, Pharm. Technol. 20 (1996) 64–74.
[31] F. Xie, S. Ji, Z. Cheng, In vitro dissolution similarity factor (f2) and in vivo bioequivalence criteria, how and when do they match? Using a BCS class II drug as a simulation example, Eur. J. Pharm. Sci. 66 (2015) 163–172. https://doi.org/10.1016/j.ejps.2014.10.002.
[32] L. Man, L. Zhen, S. Xun, G. Tao, Z. Zhirong, A polymeric prodrug of 5-fluorouracil-1-acetic acid using a multi-hydroxyl polyethylene glycol derivative as the drug carrier, PLoS One. 9 (2014). https://doi.org/10.1371/journal.pone.0112888.
[33] F. Casale, R. Canaparo, L. Serpe, E. Muntoni, C. Della Pepa, M. Costa, L. Mairone, G.P. Zara, G. Fornari, M. Eandi, Plasma concentrations of 5-fluorouracil and its metabolites in colon cancer patients, Pharmacol. Res. 50 (2004) 173–179. https://doi.org/10.1016/j.phrs.2004.01.006.
[34] Z. Dou, Y. Xu, H. Sun, Y. Liu, Synthesis of PEGylated fullerene-5-fluorouracil conjugates to enhance the antitumor effect of 5-fluorouracil, Nanoscale. 4 (2012) 4624–4630. https://doi.org/10.1039/c2nr30380a.
[35] A. Hussain, M.W. Haque, S.K. Singh, F.J. Ahmed, Optimized permeation enhancer for topical delivery of 5-fluorouracil-loaded elastic liposome using Design Expert: part II, Drug Deliv. 23 (2016) 1242–1253. https://doi.org/10.3109/10717544.2015.1124473.